Effects of Loading Rate and Normal Stress on Stress Drop and Stick-slip Recurrence Interval

Stephen L. Karner and Chris Marone

Department of Earth, Atmospheric, & Planetary Sciences, Massachusetts Institute of Technology, Cambridge, Massachusetts

In this paper we report on investigations of frictional restrengthening during repetitive stick-slip on initially bare granite surfaces (nominal contact area 25 cm^2). The tests were conducted in a double-direct shear apparatus at room-temperature and humidity. Normal stress was held constant, and shear was induced by controlling the velocity of a loading piston. Samples exhibited quasi-periodic stick-slip instabilities. Appreciable yielding and precursory creep occur prior to failure. Stress drop amplitudes range from 0.1 to 3.1 MPa (or 4-49% of the failure strength). We study the effects of loading rate (0.5 to 300 μm/s) and normal load (5 and 10 MPa) on stress drop and stick-slip recurrence interval. At a given loading rate, there is a positive correlation between stress drop and recurrence interval, indicating healing rates of ~4 MPa per decade increase in recurrence time. However, the combined data from all velocities show a lower rate, suggesting an apparent healing rate of ~1 MPa per decade increase in recurrence time. We find a consistent scaling between different loading rates when stress drop is compared to inter-event loading displacement. The data for all velocities delineate a single trend and show larger stress drops for greater pre-failure loading displacement. Failure strength and post-slip stress levels converge with increasing velocity. Our data indicate that stress drop and post-seismic stress levels depend on loading rate and recurrence interval in a complex way.

1. INTRODUCTION

Estimates from seismic moment-magnitude data show that stress drop increases by 1-5 MPa per decade change in earthquake recurrence time [*Kanamori and Allen*, 1986; *Scholz et al.*, 1986; *Marone et al.*, 1995]. These results indicate that faults restrengthen, or heal, during the interseismic period. Fault healing is also inferred from seismic surveys of faults that participate in earthquake rupture. *Li et al.* [1998] found that fault-zone p- and s-wave velocities increased with time after the 1992 Landers earthquake (M_w 7.3), indicating healing and consolidation of the fault zone. These observations are consistent with data from laboratory experiments performed under a wide range of conditions, which show that static friction increases as a function of contact time [e.g. *Dieterich*, 1972, 1978; *Chester and Higgs*, 1992; *Fredrich and Evans*, 1992; *Marone and Kilgore*, 1993; *Beeler et al.*, 1994; *Karner et al.*, 1997; *Nakatani and Mochizuki*, 1996; *Marone*, 1998a; *Karner and Marone*, 1998; *Richardson and Marone*, 1999]. However, the relationship between seismic estimates of earthquake stress drop and laboratory measurements of healing and static friction is poorly understood. Hence, it is important to investigate the mechanics of healing and the relationship between healing and frictional instability. This may be achieved by analyzing stick-slip instabilities observed from laboratory experiments.

To investigate the repetitive stick-slip behavior of rock friction, and to study the effects of loading conditions on

GeoComplexity and the Physics of Earthquakes
Geophysical Monograph 120

fault healing, we have sheared samples of initially bare rock surfaces. We find that stress drop amplitude is dependent on velocity, normal stress, recurrence interval and effective stiffness. Our results are consistent with those of previous laboratory studies, in that stress drop increases with greater normal stress and slower loading rates. The frequency of stick-slip events depends inversely on velocity via a power-law relationship. When cast in terms of recurrence time, we observe two rates at which stress drop increases with interseismic interval. The first is given by inverse loading rate such that slower velocities yield longer recurrence times and larger stress drop. A second, higher rate occurs for a given velocity and is determined by stochastic variations in fault strength between instabilities coupled with the finite elastic stiffness of the sample assembly. We analyze our data in terms of rate- and state-dependent friction constitutive laws, and we find that the model predictions capture the major features. Our results highlight the importance of accounting for variations in earthquake recurrence interval in studies of the seismic cycle and earthquake source characteristics.

2. THE EXPERIMENTS

Experiments were conducted on samples of Westerly Granite, at room-temperature and humidity, in a hydraulically driven double-direct shear testing apparatus [described by *Karner and Marone*, 1998; *Mair and Marone*, 1999]. Samples consisted of a triple-block geometry where a central forcing block is sheared between two stationary side blocks (e.g. the inset shown in Figure 1a). Samples were machined to produce side blocks with dimensions of 5x5x3 cm^3, and a central sliding block of 5x8x4 cm^3. Hence, the nominal contact area on which shear occurred was 5x5 cm^2. The same forcing blocks were used for each test, and surface roughness was controlled by machining with a #100 grinding wheel (rms roughness of ~5μm).

For each experiment, normal stress was maintained constant by controlling the loadforce signal in a servo-controlled feedback loop (resolution better than 0.1 kN). Shear was induced by controlling the velocity of the piston loading the central block of the sample assembly (control step-size of 0.1 μm/s). We monitored the applied forces and displacements with sampling rates up to 1000 Hz. The parameters that were investigated included loading rate (0.5 to 300 μm/s) and normal stress (5 or 10 MPa). To study the effects of velocity on stick-slip behavior, we imposed step changes in loading rate throughout each test. Several tens of stick-slip cycles occurred for each velocity step (up to ~70 cycles), and between 400 to 500 instabilities were recorded for the 3 cm of slip accommodated by our sample dimensions. We have analyzed each stick-slip event, and we compare our data to both previous laboratory studies and numerical simulations using existing rate- and state-dependent friction laws.

3. RESULTS

3.1. Characteristics of Repetitive Stick-slip

We show a portion of data for one experiment, including the initial load-up from zero shear stress, in Figures 1 and 2. For this test, normal stress was held constant (10 MPa) and loadpoint velocity was varied from 10 to 300 μm/s. In Figure 1a, we present the data as a function of time in order to better distinguish the stick-slip cycles for different loading rates. For the conditions of our experiments, samples exhibited unstable sliding, with instabilities occurring repeatedly. We observe a clear effect of loading rate on the frequency and amplitude of stick-slip instability. The data indicate that stick-slip amplitude decreases, and frequency increases with increasing loading rate.

In Figure 1b we focus on several stick-slip cycles as a function of loadpoint displacement. The data show the characteristic stick-slip behavior observed by previous researchers [e.g. *Ohnaka*, 1973; *Engelder et al.*, 1975; *Engelder and Scholz*, 1976; *Johnson and Scholz*, 1976; *Shimamoto and Logan*, 1981; *Teufel and Logan*, 1978; *Wong and Zhao*, 1990]. That is, shear stress increases quasi-linearly as sample loading proceeds, indicating an elastic stiffness of the loading column of ~0.065 MPa/μm. As deformation continues, shear stress departs from the quasi-linear trend indicating premonitory slip. Shear stress continues to increase until it reaches a peak value (τ_{max}) that corresponds to the traditional definition of static friction. During an instability, shear stress decreases to a fraction of the peak strength (τ_{min}). We define stress drop ($\Delta\tau$) as the difference between the pre-slip peak stress (τ_{max}) and the post-slip minimum stress (τ_{min}). With subsequent loading, samples continue to slide in an unstable manner as can be seen by the repeated, quasi-periodic stick-slip cycles.

In Figure 2 we show sample slip for the same segment of data shown in Figure 1. Sample slip is calculated from the measured shear force and loadpoint displacement, using the elastic stiffness obtained from apparatus calibrations (k=0.065 MPa/μm). Calculating sample slip in this way is justified by recent tests where we monitor slip directly by using transducers mounted on the sample blocks. Over long time intervals, the cumulative slip rate resembles the background loading velocity (Figure 2a). When viewed in detail (Figure 2b), samples exhibit intervals of relatively little motion (stick), followed by accelerating slip that

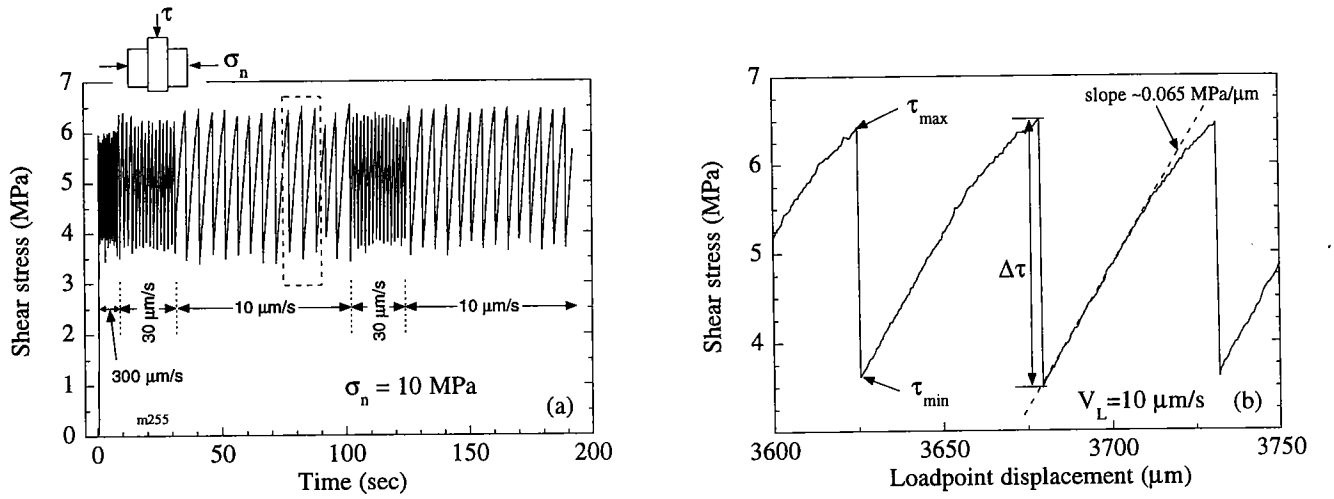

Figure 1. Shear stress data from a typical section of an experiment. **a)** Shear stress is plotted as a function of time. Loading rate was stepped between 10, 30, and 300 μm/s. Data show repeated stick-slip events, with velocity-dependent variations in stick-slip amplitude and frequency. **b)** An enlarged view of data from (a), plotted against loadpoint displacement. Loading rate for this section was 10 μm/s. For each instability, data show elastic loading with stiffness of ~0.065 MPa/μm (expressed as shear stress per unit loadpoint displacement), followed by yielding and failure.

culminates in failure and rapid motion (slip instability). We define premonitory slip as the amount of motion that occurs during yielding of the sample and prior to failure (i.e. departure from the linear elastic loading curve). The recurrence interval for a given slip instability is defined as the time since the previous slip event. The data shown in Figures 1 and 2 indicate an inverse scaling of recurrence time with loading rate, inasmuch as the frequency of instabilities is greater for faster velocities.

3.2. Relationship Between Velocity and Recurrence Interval

It is important to note that recurrence interval is not directly controlled in our experiments. However, we find that recurrence interval is dependent on loading rate, which is a control parameter. In Figure 3, we show the association between loading rate (V_L) and recurrence time (t_r) for stick-slip cycles where normal stress was 10 MPa. The imposed loading rate is the primary control for the length of time between slip events, with slower velocities resulting in longer recurrence intervals. The data indicate a relationship that is described by a power-law expression:

$$t_r = m\left(V_L\right)^n \qquad (1)$$

where m is a scaling constant, and n is the power-law exponent (-1.15 for our tests). For a single velocity the data show a range of recurrence times, a feature that is discussed in section 4. In the following section we present our data in terms of recurrence interval, which allows for better comparison to seismic observations. We explore the dependence of stress drop and fault strength on recurrence interval.

3.3. Dependence of Shear Stress on Recurrence Interval

We measured the stress drop amplitude for each instability and plot these against recurrence interval in Figure 4. While the data show some scatter (discussed in more detail below), there are distinct correlations between stress drop and the loading conditions. Stress drops are generally larger for tests conducted at greater normal stress. Furthermore, we observe two distinctly different healing rates that depend on the imposed loading velocity. For a given normal stress and velocities from 0.5 to 300 μm/s, stress drop is greater for slower loading rates and, hence, longer recurrence intervals (β_1 ~ 0.75-1 MPa per decade change of recurrence time). For a given velocity there is a second, larger healing rate (β_2), of ~3.5 to 4 MPa per decade change in time. Thus, the restrengthening rates for a single velocity are quite different to the overall healing rates observed for a wide range of loading rates.

Peak and minimum stresses for all stick-slip cycles are shown as a function of recurrence time in Figure 5. The

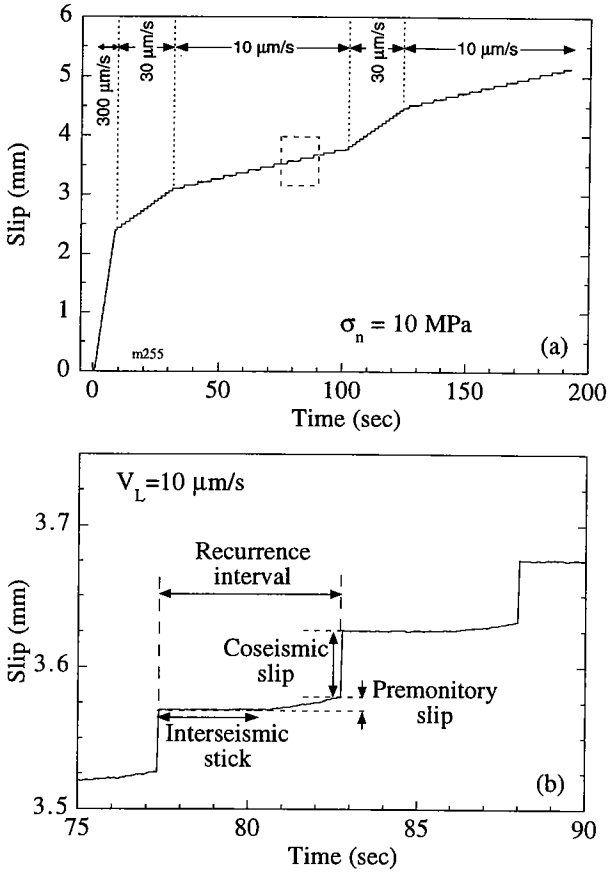

Figure 2. Cumulative slip across shear surface plotted as a function of experiment time (the same test shown in Figure 1). Slip is determined from the measured loadpoint displacement, loadforce, and elastic stiffness. **a)** The long-term slip rate closely matches the imposed loading velocity. **b)** Individual cycles show intervals of sample stick, followed by accelerating premonitory slip and instability (coseismic slip). Recurrence interval is measured from the point at which shear stress is minimum after an instability, to the point for which shear stress is maximum prior to the next instability.

data show systematic variations as a function of loading rate and normal stress. First, τ_{max} and τ_{min} are larger as normal stress increases. Second, there is a small dependence of τ_{max} and τ_{min} on loading rate. The values of τ_{max} are nearly constant, or may decrease slightly, with increasing velocity (shorter recurrence times). For a single velocity, τ_{max} increases slightly for longer recurrence intervals. Also, τ_{min} increases slightly for faster loading rates (Figure 5b). These observations are consistent with data from individual stick-slip cycles (as shown in Figure 1a), and measurements of stress drop (Figure 4).

4. DISCUSSION

4.1. Fault Healing Rates Inferred From Stress Drop Measurements

Our experiments on bare granite surfaces exhibit quasi-periodic slip instabilities, for which the amplitude and frequency are dependent on loading velocity (Figure 1). Our data show an inverse power-law relationship between loading rate and instability frequency, consistent with seismic observations of aftershock recurrence intervals [e.g. *Schaff et al.*, 1998]. Furthermore, we observe that stress drop increases logarithmically with recurrence interval, with healing rates that are consistent with earthquake data obtained from natural faults [*Kanamori and Allen*, 1986; *Cao and Aki*, 1986; *Marone et al.*, 1995]. If the healing rates observed from our experiments are taken as a measure of fault strength, then our results are comparable to previous work detailing the time-dependence of static friction [e.g. *Dieterich*, 1972, 1978; *Beeler et al.*, 1994; *Nakatani and Mochizuki*, 1996; *Marone*, 1998a; *Richardson and Marone*, 1999], and fault restrengthening inferred from seismic surveys [*Li et al.*, 1998]. However, the two different healing rates shown by our data (β_1 and β_2 in Figure 4) indicate that fault restrengthening may occur via an interplay of several processes. In order to better understand the different restrengthening rates, we first investigate the larger healing rate observed for individual velocities (β_2 in Figure 4).

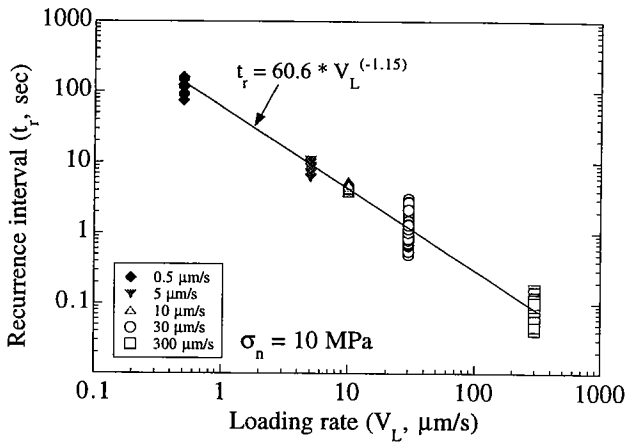

Figure 3. Recurrence interval plotted as a function of the imposed loading rate. Data are from stick-slip events occurring in three experiments for which σ_n=10 MPa and loading rates were varied from 0.5 to 300 µm/s. We observe a power law relationship between loading rate and recurrence interval.

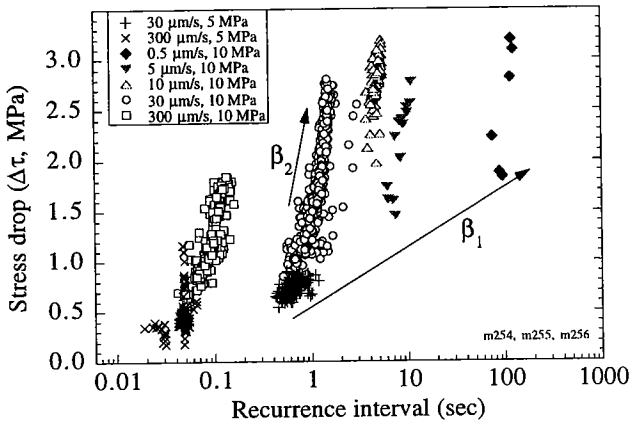

Figure 4. Measured stress drop values are shown as a function of recurrence time. Data are from the same stick-slip events shown in Figure 3, and from tests conducted at a normal stress of 5 MPa. Stress drop increases with normal load. The data show two distinct healing rates (β_1 and β_2). For a given normal load, stress drop increases by ~1 MPa per decade change in time (β_1). For a given loading rate, stress drop increases by ~4 MPa per decade change in recurrence interval (β_2). Data scatter reflects variations of material strength between stick-slip events occurring within a single experiment, and also reproducibility between experiments.

In Figure 6a, we directly compare stress drop data to recurrence interval for instabilities where V_L=30 μm/s and σ_n=10 MPa. We present data from three consecutive experiments to show data reproducibility. There is no systematic dependence of stress drop levels on the experiment order (m254, m255, and m256, consecutively). For a given experiment, the data display a range of stress drop values (~1.5 MPa, or ~75% of the range for all tests). Furthermore, we do not observe systematic variations in stress drop as a function of cumulative shear displacement or experiment time. Post-experiment observation of our samples revealed that only minor amounts of gouge had accumulated. This is important because previous studies have identified the production of wear material (gouge) as a mechanism responsible for displacement dependent friction evolution [e.g. *Byerlee*, 1967; *Marone*, 1998b]. Thus, the lack of a systematic evolution of stress drop amplitudes with displacement is consistent with the small amounts of gouge production during our tests.

The data shown in Figure 6a define a quasi-linear trend that is bounded by a line calculated from the imposed velocity and loading stiffness. This line corresponds to the loadpoint displacement between stick-slip events, and for zero precursory slip would equal the stored elastic energy. To the first order, the trend shown in Figure 6a implies that healing rates for a single velocity (β_2) are determined by the stiffness of the sample assembly. To explore this further, we present stress drop data from all instabilities in Figure 6b. Stress drop is plotted as a function of the interseismic loadpoint displacement calculated for each instability ($x=V_L t_r$). The data for all stick-slip events describe a single quasi-linear trend consistent with the loading stiffness observed from individual stick-slip cycles (k=0.065 MPa/μm, as shown in Figure 1b). Hence, this indicates that stress drop can be described in terms of loading rate, recurrence interval, and stiffness (k) by the relation:

$$\Delta\tau = V_L t_r k \qquad (2)$$

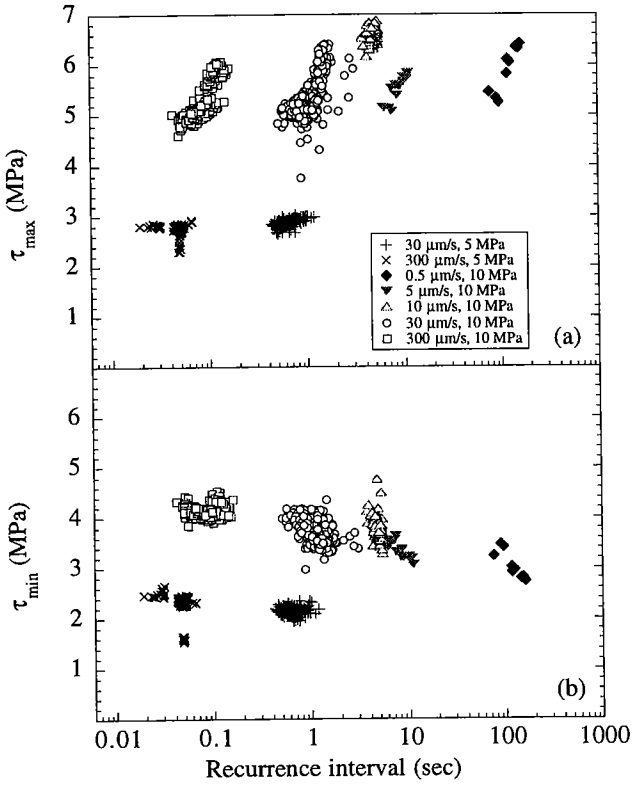

Figure 5. Shear stress data as a function of recurrence time. Data are from the same tests shown in Figure 4. **a)** Maximum shear stress prior to instability. For a given loading rate, peak stress increases with recurrence interval. For a constant normal load (i.e. including all loading rates), data show little or no dependence of peak stress on recurrence interval. **b)** Minimum stress following a slip event. Data are for the same stick-slip events shown in (a). Minimum stress increases with normal load and velocity.

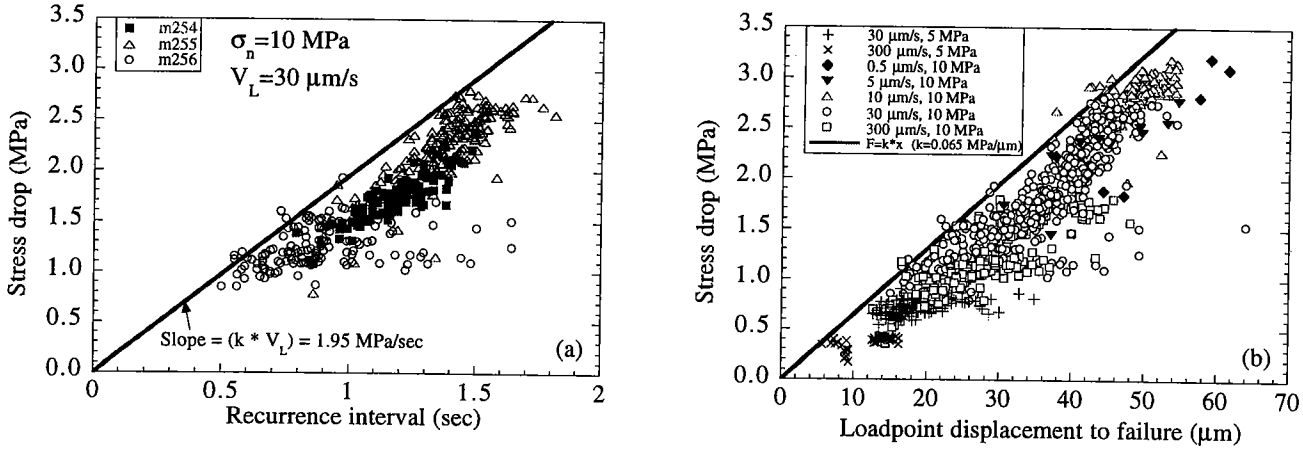

Figure 6. Stress drop data for the events shown in Figure 4. **a)** Stress drop is plotted against recurrence interval for events that occurred at the same loading conditions (i.e. σ_n=10 MPa, V_L=30 μm/s). Data from m254, m255 and m256 indicate experiment reproducibility. For a given experiment, data show a range of ~1.5 MPa in stress drop values. All data hug the calculated elastic loading curve (the line with slope kV_L, where k=0.065 MPa/μm). **b)** Stress drop data from all stick-slip events shown as a function of loadpoint displacement prior to instability. The data describe a single quasi-linear trend. For comparison to data, we show a line calculated for elastic loading of a material with stiffness of 0.065 MPa/μm. Our data hug the calculated loading curve, and consistently plot to the right of the line.

This expression can be derived from classical Coulomb theory (as shown by *Beeler and Wong*, 1999) and is consistent with data presented by other researchers [e.g. *Wong and Zhao*, 1990; *Gu and Wong*, 1991; *Berman et al.*, 1996; *Nasuno et al.*, 1998].

4.2. Second-order Variations and Data Scatter

While Equation 2 offers a first-order approximation to our data (Figure 6b), the majority of our data consistently plot to the right of the calculated linear trend. These second-order characteristics are partly due to reproducibility between experiments (as shown in Figure 6a). However, the lack of a dependence of stress drop on cumulative displacement or experiment time indicates that other factor(s) influence stick-slip behavior. For a given test, data scatter may be due to stochastic variations in strength of the sliding surfaces between slip events, or due to the effects of premonitory slip that occurs prior to instability. As the latter is consistent with our observations of yielding prior to sample failure (e.g. Figure 1b), we investigate whether stress drop is dependent on the amount of premonitory slip. We remove the linear elastic loading curve from the displacement data (see Figures 1b and 6b, Equation 2) and show the calculated values of premonitory slip in Figure 7. We do not observe any significant relationship between premonitory slip and stress drop.

The lack of a significant dependence of stress drop on premonitory slip indicates that data scatter may result from random variations in the properties of the slipping surface. As we do not control the state of the shearing surfaces between each instability, we suggest that differences in

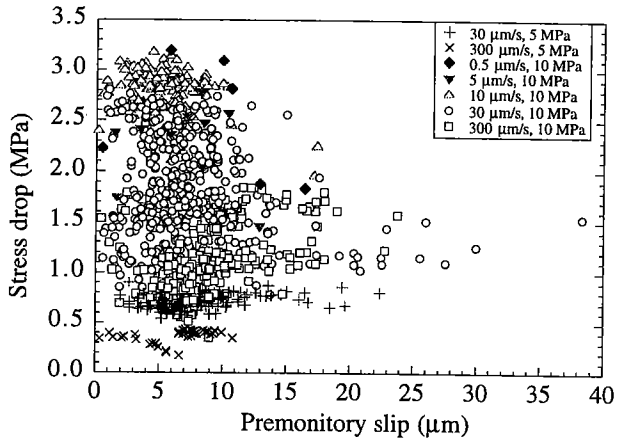

Figure 7. Stress drop shown as a function of the calculated premonitory slip to failure. Data are for the same events shown in Figure 6b. Slip is calculated as the difference between observed loadpoint displacements, and the theoretical loading curve for a stiffness of 0.065 MPa/μm. There is no systematic dependence of stress drop on pre-failure slip.

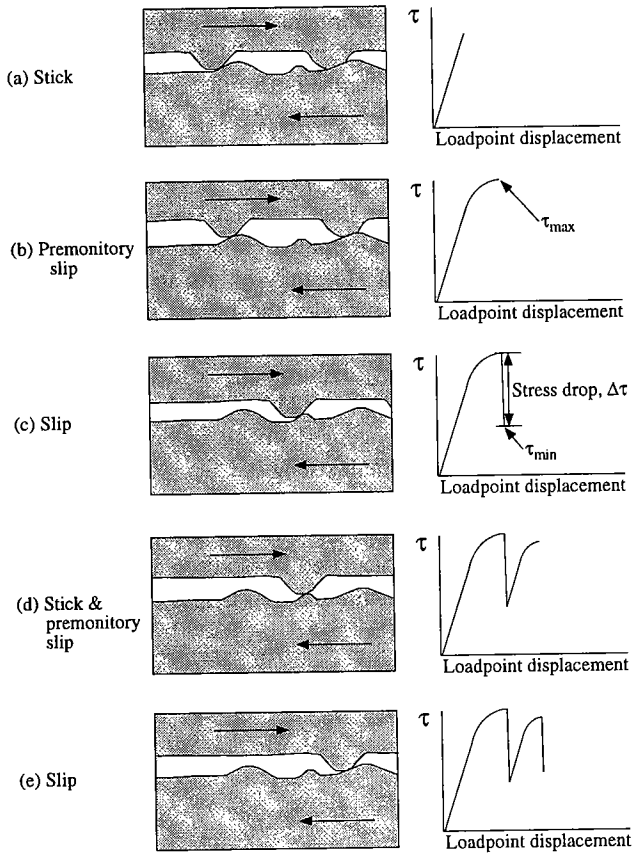

Figure 8. Schematic illustration showing how asperity contact size and population may affect shear loading behavior for stick-slip instabilities. Panels a) through e) represent consecutive snap-shots for shear on bare surfaces. The sample loads elastically with little slip (a), followed by yielding and premonitory slip (b). At failure, samples slide rapidly and exhibit a sharp reduction in shear load (c). Stick-slip cycles occur repeatedly (d-e). Peak strength and stress drop are affected by the characteristics of the asperity population.

surface evolution between stick-slip cycles may account for the stochastic character of our data. This may arise from slip and/or time dependent variations in the population and character (e.g. shape, strength) of contacting asperities, as shown schematically in Figure 8. For example, a population of strong asperities would raise the material failure strength, and inhibit premonitory slip (thus, samples would exhibit less yielding). If the number of strong asperities differed between cycles, then premonitory slip, failure strength and, perhaps, stress drop would also vary.

Other micromechanical processes may account for the variability within our data. For example, gradual deformation of contacting asperities during loading (e.g. by brittle failure) would relieve some of the imposed shear load and lead to greater premonitory slip and longer recurrence intervals. Alternately, during dynamic slip the characteristics of an asperity population may have an influence on the level of dynamic overshoot before slip is arrested. Detailed studies of surface interactions may determine which of these mechanisms is responsible for the second-order variations shown by our data. However, such work is beyond the scope of this paper.

4.3. Modeling of Data Using Rate- and State-dependent Friction Laws

We compare our data with results from forward models using existing rate- and state-dependent friction constitutive laws. For the simulations we used the Dieterich (or slowness) form of the friction evolution law [*Dieterich*, 1979], where friction (μ) at slip rate (V) is described by:

$$\mu = \mu_0 + a\ln\left(\frac{V}{V_0}\right) + b\ln\left(\frac{V_0\theta}{D_c}\right) \tag{3}$$

Here, μ_0 is steady-state sliding friction at a reference velocity (V_0), D_c is the critical slip distance, a and b are empirical scaling constants. The state variable (θ) evolves via the relation:

$$\frac{d\theta}{dt} = 1 - \left(\frac{V\theta}{D_c}\right) \tag{4}$$

Equations (3) and (4) are coupled with an expression describing the elastic interaction between the sliding surface and the testing apparatus: $d\mu/dt = k(V_l - V)$, where k is the system stiffness and V_l is the velocity of the loading piston.

The numerical simulations have been conducted for the boundary conditions of our experiments ($0.5 < V_L < 300$ μm/s), and using friction parameters (a, b, and D_c) such that the critical stiffness equals the system stiffness (0.0065 change in friction per μm, determined from stiffness value shown in Figure 1b and σ_n=10 MPa) via the relation:

$$k = K_c = \frac{(b-a)}{D_c} \tag{5}$$

To model oscillating instabilities, we perturb the numerical system by including a small slide-hold-slide (hold time of 0.0002 s) early in the simulations. The model results show frictional behavior similar to the stick-slip

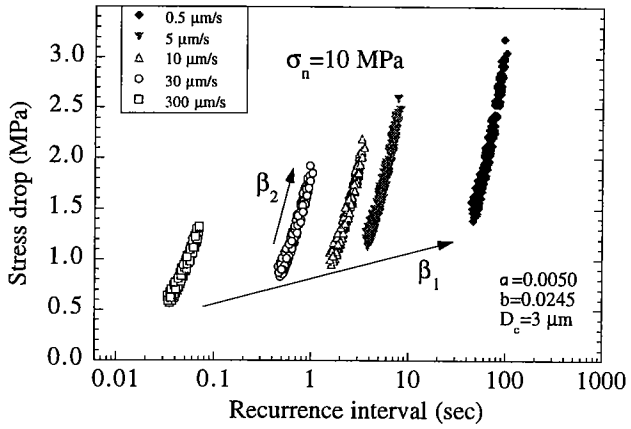

Figure 9. Results from numerical simulations using rate- and state- dependent friction laws. Simulations are forward models using the Dieterich (or slowness) law with constitutive parameters as shown. To simulate physical changes of the contacting surfaces, the state variable was randomly perturbed by a small amount (±2.5%) in the middle of each slip instability. Stress drop amplitudes are plotted as a function of recurrence interval. Results display two rates of increase in stress drop amplitudes as a function of recurrence time, consistent with our laboratory observations.

instabilities observed in our experiments. However, the simulations predict perfectly periodic behavior where stress drop amplitudes and recurrence intervals are constant with increasing slip. This is because state evolution is the same for each stick-slip cycle, which may not be the case in our experiments. Hence, to investigate the relationship between stress drop and recurrence interval we randomly perturb the state variable by a small amount (between ±2.5% of the value of state at τ_{max}) in the middle of each slip instability. This procedure is justified by physical models in which the nature of the sliding surfaces varies during stick-slip (e.g. due to wear and asperity fracturing). In such models, the greatest variability in surface characteristics would likely occur during dynamic slip. A key feature of the perturbation in state is that it yields a range of stick-slip recurrence intervals and stress drops, as we observe experimentally.

Results from these forward models are presented in Figures 9-11. We show the calculated stress drop amplitudes for instabilities in Figure 9, and the associated τ_{max} and τ_{min} values in Figure 10. The model predictions capture the first order observations from our experiments. That is, the frequency of instability (i.e. recurrence interval) is strongly dependent on the imposed loading rate (similar to Figure 3, and Equation 1). The calculated stress drop amplitudes show two distinct restrengthening rates (Figure 9), consistent with our laboratory data (Figure 4). The simulations show greater healing rates for a single velocity than for all velocities combined. Furthermore, the model predictions show little dependence of τ_{max} on loading rate and that τ_{min} increases with increasing velocity (Figure 10), consistent with our data (i.e. Figure 5). However, for a given loading rate we note that the model predictions show a greater range of τ_{min} and a smaller range for τ_{max} than that observed from our data. This may be due to the fact that the simulations do not consider the effects of inertia and neglect radiated energy. Furthermore, the simulations predict less scatter for τ_{max} than for τ_{min} which differs from our laboratory observations. This may be due to the dependence of τ_{max} on system stiffness, or on second-order variations in pre-failure fault strength.

As is the case for our laboratory data, we find that the numerically determined healing rates are well described by Equation 2. When the calculated stress drop amplitudes are compared to the interseismic loading displacement (Figure

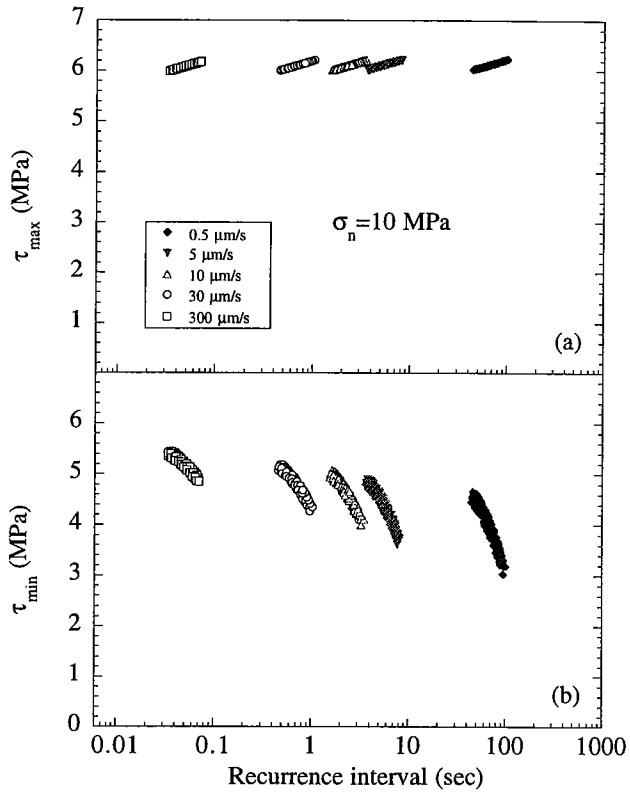

Figure 10. Calculations of τ_{max} and τ_{min} for the same numerical simulations shown in Figure 9, plotted as a function of recurrence interval. **a)** For a given loading rate, peak stress levels (prior to instability) increase slightly with recurrence time, while for **b)** minimum stress levels (after instability) decrease with recurrence interval.

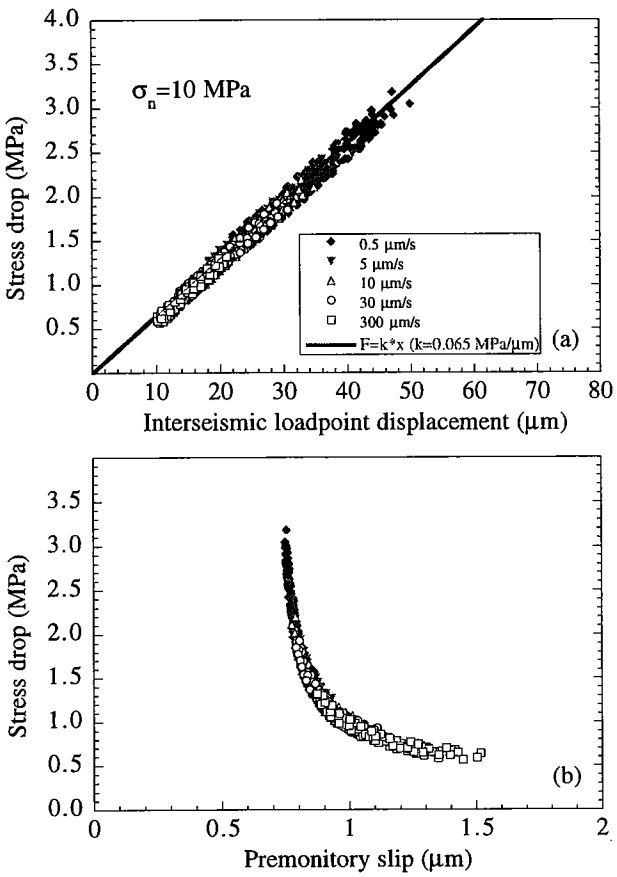

Figure 11. **a)** For comparison to our experiment results, we show stress drop amplitudes from simulations (same as those presented in Figure 9) plotted against loadpoint displacement prior to failure. Stress drop amplitudes plot as a single line that is well described by an elastic loading curve. **b)** Model calculations of stress drop plotted as a function of premonitory slip. Results show an inverse relationship between stress drop and premonitory slip, and that premonitory slip is small compared to our experiment data.

11a), the predicted values describe a single line with a slope given by the system stiffness (compare with Figure 6b). The scatter predicted by the models is consistent with data from our experiments, suggesting that stochastic evolution of state is a plausible explanation of our experimental observations. However, we note that the amount of scatter predicted by the models is less than that shown by our laboratory data. This may arise from differences between the observed and modeled amounts of premonitory slip. Model calculations of premonitory slip are shown in Figure 11b. The simulations show less premonitory slip than observed from our experiments, and an inverse relationship between slip and stress drop. While our data do not show a dependence of stress drop on premonitory slip (compare Figures 11b and 7), it may be that such a relationship is masked by the data scatter. The larger values of premonitory slip and the greater amount of scatter observed from our laboratory measurements may result from stochastic variations of the state of the sliding surface during the yielding phase prior to failure.

4.4. Comparison to Previous Studies

4.4.1 Seismic Observations. Our results are consistent with seismic observations, inasmuch as inter-event recurrence interval scales inversely with loading rate [e.g. *Schaff et al.*, 1998], and that stress drop increases with longer recurrence intervals [*Kanamori and Allen*, 1986; *Marone et al.*, 1995] and with slower loading rates [*Cao and Aki*, 1986]. Furthermore, our data show a range of recurrence intervals and stress drop values for a given velocity, also consistent with seismic observations [*Cao and Aki*, 1986]. By reanalyzing the data of *Kanamori and Allen* [1986] in terms of velocity, *Cao and Aki* [1986] found that stress drop values exhibited considerable scatter for a given loading rate. From this they reasoned that fault strength is affected by heterogeneities in the number of strong asperities. If variations in asperity geometry and strength are also considered, then such a micromechanical model would account for the stochastic nature of our room temperature data.

We recognize that the conditions at hypocentral depths introduce other factors that could influence fault healing rates and stress drop levels. Laboratory studies have explored several of these factors - including temperature, fluid-rock interactions, and variations in stress state [e.g. *Chester and Higgs*, 1992; *Linker and Dieterich*, 1992; *Fredrich and Evans*, 1992; *Karner et al.*, 1997; *Nakatani*, 1998; *Karner and Marone*, 1998; *Richardson and Marone*, 1999]. As it is unlikely for every fault to experience the same physico-chemical conditions, variations in these parameters may account for some scatter observed from seismic data. However, the conditions at hypocentral depths provide added complexity which must be separated from the purely physical mechanisms that effect fault healing (such as loading rate).

4.4.2. Laboratory Data. Our data show that stress drop decreases with increasing loading rates (i.e. lower recurrence times, Figures 1 and 4), in agreement with results from previous studies of frictional instability for geologic materials [*Ohnaka*, 1973; *Engelder et al.*, 1975; *Engelder and Scholz*, 1976; *Johnson and Scholz*, 1976; *Shimamoto and Logan*, 1981; *Teufel and Logan*, 1978; *Wong and Zhao*,

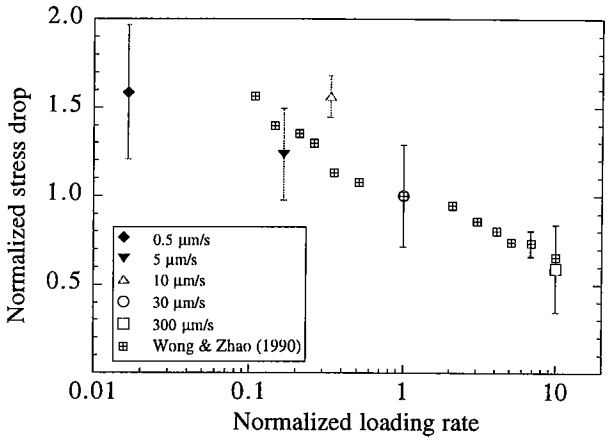

Figure 12. Our stress drop data are plotted with data from *Wong and Zhao* [1990]. For comparison, we normalize our data by the mean value for a loading rate of 30 μm/s (1.8 MPa). Velocities are normalized by 30 μm/s. We present our data as mean and standard deviation for each normalized velocity, and we show the maximum uncertainty presented by *Wong and Zhao* [1990]. Our results are consistent with those of *Wong and Zhao* [1990], with a similar inverse scaling between stress drop and loading rate.

1990], for metals [*Rabinowicz*, 1958], and for thin molecular films separating sheets of mica [*Berman et al.*, 1996]. *Wong and Zhao* [1990] presented stick-slip data from experiments conducted in a triaxial deformation apparatus at normal stresses from 25 to 250 MPa. They performed velocity-stepping tests on fine-grained quartz gouge sandwiched between Westerly granite forcing blocks. They averaged the data for each velocity step, and presented the results as the ratio between consecutive velocity groups. Hence, their data were essentially normalized by reference values of loading velocity, stress drop, and recurrence interval. To remain consistent with *Wong and Zhao* [1990] and to assist with comparison, we have normalized our stress drop and loading rate data by reference values (corresponding to the mean stress drop of ~1.8 MPa at a velocity of 30 μm/s). We present a comparison between our data, and those of *Wong and Zhao* [1990] in Figure 12. The inverse relationship that we observe between stress drop and loading rate are in agreement with the data of *Wong and Zhao* [1990]. Furthermore, *Wong and Zhao* [1990] observed that their normalized stress drop levels increased with normalized recurrence interval, which is consistent with the results of this study.

Berman et al. [1996] also investigated the effects of loading rate on stick-slip behavior from experiments conducted on thin molecular films sandwiched between mica surfaces. As a function of increasing velocity, they observed that static friction levels decreased and post-failure minimum friction increased. Their data define a critical velocity (V_c) above which stick-slip motion transitioned to continuous stable sliding (V_c ~ 7 to 8 μm/s for their tests). A similar critical velocity has been observed from dry friction experiments on bristol board and also on paper [*Baumberger et al.*, 1994; *Heslot et al.*, 1994]. These researchers observed a transition from stick-slip to stable sliding that depends on loading rate and stiffness. Their data showed that stable sliding is promoted by both increased stiffness and increased velocity. In the vicinity of the bifurcation of slip behavior, they also found that frictional characteristics differed significantly for low and high loading rates. From these observations, they identified that the low velocity regime was creep dominated and could be defined by a characteristic length scale, while the high velocity regime was inertia dominated and has a characteristic time scale. Hence, the combined results of *Berman et al.* [1996], *Baumberger et al.* [1994], and *Heslot et al.* [1994] indicate that stiffness and loading rate can effect the behavior of stick-slip motion and the transition to stable sliding.

To compare with the study of *Berman et al.* [1996], we show in Figure 13b the levels of peak stress (τ_{max}) and post-slip minimum stress (τ_{min}) from our tests as a function of loading rate, and for a constant normal stress of 10 MPa. The data show that τ_{max} decreases slightly with loading rate, while τ_{min} increases with velocity. Hence, τ_{max} and τ_{min} converge with faster loading rates, consistent with the observations of *Berman et al.* [1996]. For the conditions of our experiments, and in light of the results of *Berman et al.* [1996], *Baumberger et al.* [1994], and *Heslot et al.* [1994], our data suggest that a critical velocity exists above which stable sliding may be achieved. This would correspond to a Hopf bifurcation between unstable and stable sliding at a fast loading rate, similar to those reported previously [*Klein et al.*, 1997; *Scholz*, 1998]. Given that this critical velocity would be large (>1000 μm/s), we suggest that the transition from stick-slip to stable sliding would occur in an inertia-dominated regime. To date, we have not observed this bifurcation, which may occur at a velocity greater than we can presently achieve with our testing apparatus. However, we have observed a similar velocity-dependent convergence of τ_{max} and τ_{min} from shear tests on layers of soda-lime glass beads [*K. Frye*, personal communication]. The existence of this transition in sliding behavior may have implications for studies of earthquake mechanics and models of rupture dynamics.

5. SUMMARY

To study stick-slip behavior of bare rock surfaces, we have conducted experiments on Westerly granite in a biaxial

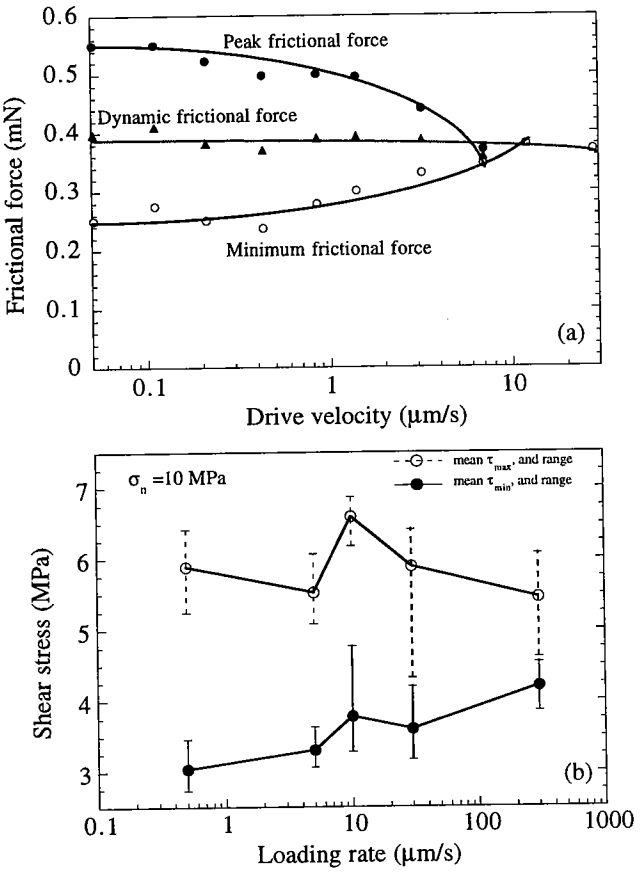

Figure 13. Peak and minimum stress levels shown as a function of loading rate. **a)** Data from *Berman et al.* [1996] showing measured peak, dynamic, and minimum frictional force from stick-slip instabilities for tests on thin molecular films between mica surfaces. Their data show convergence of peak and minimum stress levels as a function of loading rate. Above a critical velocity (~8 μm/s), they observe a transition to stable sliding. **b)** Shear stress data from our experiments as a function of loading rate. For clarity, we show the mean value and range of shear stress data for each velocity. For faster velocities, τ_{min} increases and τ_{max} decreases slightly. Thus, peak and minimum stress levels converge as velocity increases similar to results from *Berman et al.* [1996].

apparatus at room-temperature and humidity. We have analyzed over 1500 instabilities, and the data show several interesting features. We observe that stress drop amplitude increases with greater normal stress, consistent with previous studies. We also observe two apparent rates of restrengthening. For a single loading rate, stress drop increases by ~4 MPa per decade in recurrence time. The combined data from all velocities show that stress drop increases by ~1 MPa per decade in time. For the conditions of our tests, this discrepancy in restrengthening rates can be characterized in terms of stiffness of the loading column, loading rate, and recurrence interval. After removing elastic effects, we do not observe any systematic dependence of stress drop on premonitory slip. Measurements of pre-failure peak stress, and post-failure minimum stress, show convergence with faster loading rates. This is consistent with previous studies that identify a critical velocity marking a transition between stick-slip and stable sliding, and that this transition lies in an inertia-dominated regime. Our results are important for studies of the seismic cycle and modeling of earthquake source characteristics, as stress drop depends not only on loading rate but also on stochastic variations in earthquake recurrence times.

Acknowledgments. This research was supported by NSF Grant EAR-9627895 and by USGS Grant 99HQGR0003. We thank the anonymous reviewers for their constructive comments and thoughtful suggestions about this manuscript. We are also grateful to K. Frye, K. Mair, U. Mok, E. Richardson and J. Renner for their stimulating discussions about this work.

REFERENCES

Baumberger, T., Heslot, F., and Perrin, B., Crossover from creep to inertial motion in friction dynamics, *Nature*, 367, 544-546, 1994.

Beeler, N.M., Hickman, S.H., and Wong, T-f., Earthquake stress drop and laboratory inferred interseismic strength recovery, *Manuscript in preparation.*

Beeler, N.M., Tullis, T.E., and Weeks, J.D, The roles of time and displacement in the evolution effect in rock friction, *Geophys. Res. Lett.*, 21, 1987-1990, 1994.

Berman, A.D., Ducker, W.A., and Israelachvili, J.N., Experimental and theoretical investigations of stick-slip friction mechanisms, In *Physics of Sliding Friction*, Edited by B.N.J. Perrson and E. Tossatti, Kluwer Academic Publ., Netherlands, 1996.

Byerlee, J.D., Frictional characteristics of granite under high confining pressure, *J. Geophys. Res.*, 72, 3639-3648, 1967.

Cao, T., and Aki, K., Effect of slip rate on stress drop, *Pageoph.*, 515-529, 1986.

Chester, F.M., and Higgs, N.G., Multimechanism friction constitutive model for ultrafine quartz gouge at hypocentral conditions, *J. Geophys. Res.*, 97, 1857-1870, 1992.

Dieterich, J.H., Time-dependent friction in rocks, *J. Geophys. Res.*, 77, 3690-3697, 1972.

Dieterich, J.H., Time-dependent friction and the mechanics of stick-slip, *Pure Appl. Geophys.*, 116, 790-805, 1978.

Dieterich, J.H., Modeling of rock friction 1: Experimental results and constitutive equations, *J. Geophys. Res.*, 84, 2161-2168, 1979.

Engelder, J.T., Logan, J.M., and Handin, J., The sliding characteristics of sandstone on quartz fault-gouge, *Pure Appl. Geophys.*, 113, 69-86, 1975.

Engelder, J.T., and Scholz, C.H., The role of asperity indentation and ploughing in rock friction II, *Int. J. Rock Mech. Mining Sci. Geomech. Abstr., 13, 155-163, 1976.*, 113, 69-86, 1976.

Fredrich, J.T., and Evans, B., Strength recovery along simulated faults by solution transfer processes, *Proc. 33rd Natl. Rock Mech. Symp.*, ed. W. Wawersik, 121-130, Rotterdam: Balkema, 1992.

Gu, Y. and Wong, T-f., Effects of loading velocity, stiffness and inertia on the dynamics of a single degree of freedom spring-slider system, *J. Geophys. Res.*, 96, 21677-21691, 1991.

Heslot, F., Baumberger, T., Perrin, B., Caroli, B., and Caroli, C., Creep, stick-slip, and dry-friction dynamics: Experiments and a heuristic model, *Phys. Rev. E*, 49, 4973-4988, 1994.

Johnson, T.L., and Scholz, C.H., Dynamic properties of stick-slip friction of rocks, *J. Geophys. Res.*, 81, 881-889, 1976.

Kanamori, H., and Allen, C.R., Earthquake repeat time and average stress drop, In *AGU Geophys. Mono. Vol. 37*, Edited by S. Das, J. Boatwright & C.H. Scholz, 227-236, 1986.

Karner, S.L., and Marone, C., The effect of shear load on frictional healing in simulated fault gouge, *Geophys. Res. Lett.*, 25, 4561-4564, 1998.

Karner, S.L., Marone, C., and Evans, B., Laboratory study of fault healing and lithification in simulated fault gouge under hydrothermal conditions, *Tectonophysics*, 277, 41-55, 1997.

Klein, W., Rundle, J.B., and Ferguson, C.D., Scaling and nucleation in models of earthquake faults, *Phys. Rev. Lett.*, 78, 3793-3796, 1997.

Li, Y-g, Vidale, J.G, Aki, K., Xu, F., and Burdette, T., Evidence of shallow fault zone strengthening after the 1992 M7.5 Landers, California, earthquake, *Science*, 279, 217-220, 1998.

Linker, M.F., and Dieterich, J.H., Effects of variable normal stress on rock friction: observations and constitutive equations, *J. Geophys. Res.*, 97, 4923-4940, 1992.

Mair, K., and Marone, C., Friction of simulated fault gouge at a wide range of velocities and variable normal stresses, *J. Geophys. Res.*, 1999, In press.

Marone, C., The effect of loading rate on static friction and the rate of fault healing during the earthquake cycle, *Nature*, 391, 69-72, 1998a.

Marone, C., Laboratory-derived friction laws and their application to seismic faulting, *Annu. Rev. Earth Planet. Sci.*, 26, 643-696, 1998b.

Marone, C., and Kilgore, B., Scaling of the critical slip distance for seismic faulting with shear strain in fault zones, *Nature*, 362, 618-621, 1993.

Marone, C., Vidale, J.E., and Ellsworth, W., Fault healing inferred from time dependent variations in source properties of repeating earthquakes, *Geophys. Res. Lett.*, 22, 3095-3098, 1995.

Nakatani, M., A new mechanism of slip-weakening and strength recovery of friction associated with the mechanical consolidation of gouge, *J. Geophys. Res.*, 103, 27239-27256, 1998.

Nakatani, M., and Mochizuki, H., Effects of shear stress applied to surface in stationary contact on rock friction, *Geophys. Res. Lett.*, 23, 869-872, 1996.

Nasuno, S., Kudrolli, A., Bak, A., and Gollub, J.P., Time-resolved studies of stick-slip friction in sheared granular layers, *Phys. Rev. E*, 58, 2161-2171, 1998.

Ohnaka, M., Experimental studies of stick-slip and their application to the earthquake source mechanism, *J. Phys. Earth*, 21, 285-303, 1973.

Rabinowicz, E., The intrinsic variables affecting the stick-slip process, *Proc. Phys. Soc. London*, 71, 668-675, 1958.

Richardson, E., and Marone, C., Effects of normal stress vibrations on frictional healing, *J. Geophys. Res.*, 1999, In press.

Schaff, D.P., Beroza, G.C., and Shaw, B.E., Postseismic response of repeating aftershocks, *Geophys. Res. Lett.*, 25, 4549-4552, 1998.

Scholz, C.H., Earthquakes and friction laws, *Nature*, 391, 37-42, 1998.

Scholz, C.H., Aviles, C.A., and Wesnousky, S.G., Scaling differences between large interplate and intraplate earthquakes, *Bull. Seismol. Soc. Am.*, 76, 65-70, 1986.

Shimamoto, T., and Logan, J.M., Effects of simulated fault gouge on the sliding behavior of Tennessee sandstone: nonclay gouges, *J. Geophys. Res.*, 86, 2902-2914, 1981.

Teufel, L.W., and Logan, J.M., Effect of displacement rate on the real area of contact and temperature generated during frictional sliding of Tennessee sandstone, *Pure Appl. Geophys.*, 116, 840-872, 1978.

Wong, T-f., and Zhao, Y., Effects of loadpoint velocity on frictional instability behavior, *Tectonophys.*, 175, 177-195, 1990.

S.L. Karner (corresponding author) and C. Marone, Department of Earth, Atmospheric and Planetary Science (54-720), Massachusetts Institute of Technology, 77 Massachusetts Ave., Cambridge, MA, USA, 02139

Engelder, J.T., and Scholz, C.H., The role of asperity indentation and ploughing in rock friction II, *Int. J. Rock Mech. Mining Sci. Geomech. Abstr., 13, 155-163, 1976.*, 113, 69-86, 1976.

Fredrich, J.T., and Evans, B., Strength recovery along simulated faults by solution transfer processes, *Proc. 33rd Natl. Rock Mech. Symp.*, ed. W. Wawersik, 121-130, Rotterdam: Balkema, 1992.

Gu, Y. and Wong, T-f., Effects of loading velocity, stiffness and inertia on the dynamics of a single degree of freedom spring-slider system, *J. Geophys. Res.*, 96, 21677-21691, 1991.

Heslot, F., Baumberger, T., Perrin, B., Caroli, B., and Caroli, C., Creep, stick-slip, and dry-friction dynamics: Experiments and a heuristic model, *Phys. Rev. E*, 49, 4973-4988, 1994.

Johnson, T.L., and Scholz, C.H., Dynamic properties of stick-slip friction of rocks, *J. Geophys. Res.*, 81, 881-889, 1976.

Kanamori, H., and Allen, C.R., Earthquake repeat time and average stress drop, In *AGU Geophys. Mono. Vol. 37*, Edited by S. Das, J. Boatwright & C.H. Scholz, 227-236, 1986.

Karner, S.L., and Marone, C., The effect of shear load on frictional healing in simulated fault gouge, *Geophys. Res. Lett.*, 25, 4561-4564, 1998.

Karner, S.L., Marone, C., and Evans, B., Laboratory study of fault healing and lithification in simulated fault gouge under hydrothermal conditions, *Tectonophysics*, 277, 41-55, 1997.

Klein, W., Rundle, J.B., and Ferguson, C.D., Scaling and nucleation in models of earthquake faults, *Phys. Rev. Lett.*, 78, 3793-3796, 1997.

Li, Y-g, Vidale, J.G, Aki, K., Xu, F., and Burdette, T., Evidence of shallow fault zone strengthening after the 1992 M7.5 Landers, California, earthquake, *Science*, 279, 217-220, 1998.

Linker, M.F., and Dieterich, J.H., Effects of variable normal stress on rock friction: observations and constitutive equations, *J. Geophys. Res.*, 97, 4923-4940, 1992.

Mair, K., and Marone, C., Friction of simulated fault gouge at a wide range of velocities and variable normal stresses, *J. Geophys. Res.*, 1999, In press.

Marone, C., The effect of loading rate on static friction and the rate of fault healing during the earthquake cycle, *Nature*, 391, 69-72, 1998a.

Marone, C., Laboratory-derived friction laws and their application to seismic faulting, *Annu. Rev. Earth Planet. Sci.*, 26, 643-696, 1998b.

Marone, C., and Kilgore, B., Scaling of the critical slip distance for seismic faulting with shear strain in fault zones, *Nature*, 362, 618-621, 1993.

Marone, C., Vidale, J.E., and Ellsworth, W., Fault healing inferred from time dependent variations in source properties of repeating earthquakes, *Geophys. Res. Lett.*, 22, 3095-3098, 1995.

Nakatani, M., A new mechanism of slip-weakening and strength recovery of friction associated with the mechanical consolidation of gouge, *J. Geophys. Res.*, 103, 27239-27256, 1998.

Nakatani, M., and Mochizuki, H., Effects of shear stress applied to surface in stationary contact on rock friction, *Geophys. Res. Lett.*, 23, 869-872, 1996.

Nasuno, S., Kudrolli, A., Bak, A., and Gollub, J.P., Time-resolved studies of stick-slip friction in sheared granular layers, *Phys. Rev. E*, 58, 2161-2171, 1998.

Ohnaka, M., Experimental studies of stick-slip and their application to the earthquake source mechanism, *J. Phys. Earth*, 21, 285-303, 1973.

Rabinowicz, E., The intrinsic variables affecting the stick-slip process, *Proc. Phys. Soc. London*, 71, 668-675, 1958.

Richardson, E., and Marone, C., Effects of normal stress vibrations on frictional healing, *J. Geophys. Res.*, 1999, In press.

Schaff, D.P., Beroza, G.C., and Shaw, B.E., Postseismic response of repeating aftershocks, *Geophys. Res. Lett.*, 25, 4549-4552, 1998.

Scholz, C.H., Earthquakes and friction laws, *Nature*, 391, 37-42, 1998.

Scholz, C.H., Aviles, C.A., and Wesnousky, S.G., Scaling differences between large interplate and intraplate earthquakes, *Bull. Seismol. Soc. Am.*, 76, 65-70, 1986.

Shimamoto, T., and Logan, J.M., Effects of simulated fault gouge on the sliding behavior of Tennessee sandstone: nonclay gouges, *J. Geophys. Res.*, 86, 2902-2914, 1981.

Teufel, L.W., and Logan, J.M., Effect of displacement rate on the real area of contact and temperature generated during frictional sliding of Tennessee sandstone, *Pure Appl. Geophys.*, 116, 840-872, 1978.

Wong, T-f., and Zhao, Y., Effects of loadpoint velocity on frictional instability behavior, *Tectonophys.*, 175, 177-195, 1990.

S.L. Karner (corresponding author) and C. Marone, Department of Earth, Atmospheric and Planetary Science (54-720), Massachusetts Institute of Technology, 77 Massachusetts Ave., Cambridge, MA, USA, 02139